

NJC

New Journal of Chemistry

Accepted Manuscript

A journal for new directions in chemistry

This article can be cited before page numbers have been issued, to do this please use: T. K. Ghosh, S. Jana, S. Jana and A. Ghosh, *New J. Chem.*, 2020, DOI: 10.1039/D0NJ03325A.



This is an Accepted Manuscript, which has been through the Royal Society of Chemistry peer review process and has been accepted for publication.

Accepted Manuscripts are published online shortly after acceptance, before technical editing, formatting and proof reading. Using this free service, authors can make their results available to the community, in citable form, before we publish the edited article. We will replace this Accepted Manuscript with the edited and formatted Advance Article as soon as it is available.

You can find more information about Accepted Manuscripts in the [Information for Authors](#).

Please note that technical editing may introduce minor changes to the text and/or graphics, which may alter content. The journal's standard [Terms & Conditions](#) and the [Ethical guidelines](#) still apply. In no event shall the Royal Society of Chemistry be held responsible for any errors or omissions in this Accepted Manuscript or any consequences arising from the use of any information it contains.

Tetra- and poly-nuclear Cd(II) complexes of an N₃O₄ Schiff base ligand: Crystal structures, electrical conductivity and photoswitching property

View Article Online
DOI: 10.1039/C5NJ03325A

Tanmoy Kumar Ghosh,^a Sumanta Jana,^b Subrata Jana^a and Ashutosh Ghosh^{a*}

^aDepartment of Chemistry, University College of Science, University of Calcutta, 92, A.P.C. Road, Kolkata 700 009, India, E-mail address: ghosh_59@yahoo.com

^bDepartment of Chemistry, Jadavpur University, Jadavpur, Kolkata 700032, India

Abstract

Two new Cd(II) complexes, [Cd₄L₂(NO₃)₂(μ_{1,1}-N₃)₂(CH₃OH)₂] (**1**) and {[Cd₂L(IPA)]₂·(CH₃OH)}_n (**2**) have been synthesized by using a multidentate Schiff base ligand H₂L (*N,N'*-bis(3-methoxysalicylidene)-diethylenetriamine) and two bridging co-ligands azide and isophthalic acid (IPA), respectively. Single crystal structure analysis shows that complex **1** has tetranuclear structure whereas complex **2** forms a 1D polymer. The photoswitching behavior of both complexes has been measured under 1 Sun illumination. A significant enhancement of frequency ~65 Hz was observed for complex **2** but for complex **1** no such enhancement was detected. To gain a detail understanding about charge transport mechanism of the complexes, the effective carrier mobility, transit time, carrier concentration and diffusion length have been estimated considering Schottky Barrier Diodes (SBD) characteristics. The charge transport properties of complex **2** were found to be superior to complex **1**. Complex **2** showed increased conductivity from 5.4×10⁻⁸ S cm⁻¹ to 135 × 10⁻⁸ S cm⁻¹ in the presence of light.

Introduction

Over the last few years, the scientific research based on Coordination Polymer (CP) have attracted significant attention due to not only their fascinating structural diversity but also their versatile potential applications in several fields of chemistry and materials science such as gas storage and separation, catalysis, ion exchange, drug delivery, fuel cell, barrier diode, photoelectric material, magnetism and sensing applications.¹⁻²³ Generally CPs are prepared by

the reaction of metal salts or metal-ion clusters with the multidentate bridging organic ligands.^{24,25} The structural diversity of the CPs can be tuned by altering the metal centres, the organic linkers and also by the reaction pathway.^{26,27} The potential applications of CPs by exploiting their large surface area and porosity have been studied comprehensively during the last decades but the prospect of CPs to be used as photovoltaics and optoelectronic devices is still remain unexplored to a great extent.^{28,29} The electronic properties of CPs can also be controlled by using appropriate metal ions and organic linkers like other performance of CPs.^{6,30} Recently, some literature reports showed that CPs prepared from d¹⁰ metal ions (Zn²⁺, Cd(II)) with different benzene dicarboxylate linkers have the ability to be used for the fabrication of optoelectronic devices like Schottky barrier diodes (SBD).^{16,31} A Schottky diode is a diode that has a low forward voltage drop and a very fast switching ability. It is formed by the junction of metal and semiconductor. Some CP based devices under dark and illumination conditions can show non-linear rectifying behavior i.e. behave like Schottky barrier diodes. There are several reports where CPs are successfully employed as diodes that harvest visible light and show enhanced photocurrent generation.³²⁻³⁴ Inspired by the above facts, several groups including ours have synthesized Cd(II) based CPs which exhibit photoswitching properties and electrical conductivity.³⁵⁻³⁷ The structure property relationships of the CPs have also been explored which is very important for the fabrication of these types of optoelectronic devices.

In the present work, we have synthesized two Cd^{II} complexes [Cd₄L₂(NO₃)₂(μ_{1,1}-N₃)₂(CH₃OH)₂] (**1**) and {[Cd₂L(IPA)]₂·(CH₃OH)}_n (**2**) using a multidentate Schiff base ligand H₂L (*N,N'*-bis(3-methoxysalicylidene)-diethylenetriamine) and two bridging co-ligands azide and isophthalic acid (IPA), respectively. Complex **1** possesses discrete tetranuclear structure whereas complex **2** is a one-dimensional coordination polymer (1D CP). The photo-switching behavior and electrical conductivity of both the complexes have been measured in order to comprehend and portray a proper comparison between the electrical properties of discrete multinuclear complex and a one-dimensional coordination polymer. A substantial on-off ratio (65 Hz) for photo switching behavior has been observed for complex **2** but for complex **1** no such enhancement is detected. To gain insight into the charge transport mechanism of the complexes, the effective carrier mobility, transit time, carrier concentration and diffusion length have been estimated considering Schottky barrier diodes (SBD) characteristics. An

improvement of charge transport properties has been noticed for polymeric complex **2** compared to complex **1**.

Experimental Section

Synthesis of Schiff base ligands (H₂L)

The Schiff base ligand (H₂L = *N,N'*-bis(3-methoxysalicylidene)diethylenetriamine) was synthesized in our laboratory by following the methods reported earlier.^{38,39}

Synthesis of the complex [Cd₄(L)₂(NO₃)₂(μ_{1,1}-N₃)₂(CH₃OH)₂] (**1**)

A methanolic solution (20 mL) of Schiff base ligand (1 mmol, 0.371 g) was added to a methanolic solution (15 mL) of Cd(NO₃)₂·4H₂O (2 mmol, 0.617 g) with constant stirring. Then an aqueous solution (1 mL) of sodium azide (0.065 g, 1 mmol) was added to the above mixture. The resulting solution was stirred for further 2 h and then the solution was left at open atmosphere. Diffraction quality light yellow colored single crystals were obtained after four days on slow evaporation of the solvent.

Yield: 0.511 g (70%) C₄₂H₅₄Cd₄N₁₄O₁₆ (1460.63). Calculated C, 34.54; H, 3.73; N, 13.43; Found C, 34.47; H, 3.81; N, 13.54; IR: ν_(N-H) = 3051 cm⁻¹, ν_(C=N) = 1633 cm⁻¹, ν_(N₃) = 2057 cm⁻¹, ν_(NO₃) = 1384 cm⁻¹.

Synthesis of the complex {[Cd₂(L)(IPA)]₂·(CH₃OH)}_n (**2**)

To a methanolic solution (20 mL) of Schiff base ligand (1 mmol, 0.371 g), solid Cd(NO₃)₂·4H₂O (2 mmol, 0.617 g) was added and stirred for 10 min. A solution of isophthalic acid (IPA, 0.166 g, 1 mmol) was prepared separately in 10 mL distilled water and 280 μL triethylamine (2 mmol) was added to it and mixed well. The solution was then added drop wise to the above mentioned methanolic solution and stirred for 45 min. Light yellow colored single crystals for X-ray diffraction were obtained by slow diffusion of diethyl ether into the solution.

Yield: 0.503 g (65%) C_{28.5}H₂₉Cd₂N₃O_{8.5} (774.35). Calculated C, 44.20; H, 3.77; N, 5.43; Found C, 44.30; H, 3.68; N, 5.35; IR: ν_(N-H) = 3220 cm⁻¹, ν_(C=N) = 1640 cm⁻¹, ν_(NO₃) = 1384 cm⁻¹, ν_{(s+as)(COO⁻)} = 1387, 1557 cm⁻¹.

Physical measurements

View Article Online
DOI: 10.1039/D0NJ03325A

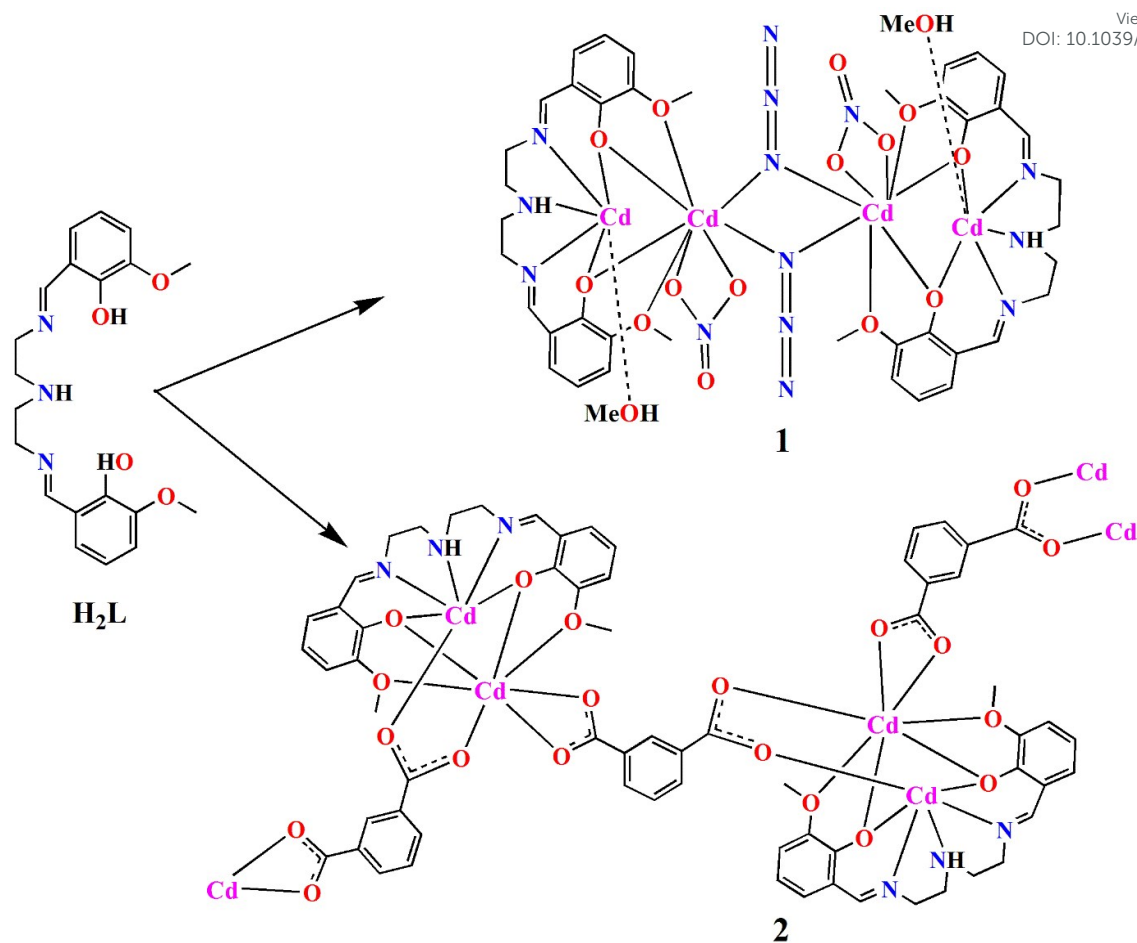
IR spectra, Elemental analyses, UV-vis spectra and Powder X-ray of complexes **1** and **2** have been performed as previously reported.^{37,39}

Thin film fabrication from the precursor complexes

In this paper thin films of precursor complexes have been synthesized onto properly cleaned ITO glass substrate (resistance $\sim 10 \Omega/\text{sq cm}$) of surface area $2.0 \text{ cm} \times 1.0 \text{ cm}$ by spin-coating of precursor solution. For the preparation of working solution, precursor complex is intimately mixed with methanol in the ratio 1:5. With the help of micro-pipette few drops of working solution were allowed to fall onto the centre of a stationary conducting ITO substrate. Then solution was spin-coated at 1500 rpm for 2 minutes and it is repeated for 3 times. The resulting film was taken out and kept in desiccators. The same procedure was repeated for capped complex precursor. The thicknesses of the film were measured to $\sim 400 \text{ nm}$ by surface profilometer (Bruker contour G).

X-ray Crystallographic data collection and refinement

Crystallographic data of single crystals of complexes **1** and **2** have been collected as previously reported.³⁹ The structure was solved by direct methods and refined by full-matrix least squares on F^2 using the Shelxl16-6 package and Olex2 program.^{40,41} Absorption corrections were carried out using the SADABS program.⁴² C10B and C11B atoms in complex **2** were disordered and was refined considering a model in which two different sites were located for the carbon atoms. Data collection, structure refinement parameters and crystallographic data for complexes **1** and **2** are given in Table 1. CCDC 1975601 1975602 contain the supplementary crystallographic data for this paper.



Scheme 1. Synthesis of complexes **1–2**.

Results and discussion

Syntheses of the complexes

The Schiff base ligand, N,N' -bis(3-methoxysalicylidene)diethylenetriamine (H_2L) was prepared following the literature method by 1:2 condensation of diethylenetriamine and *o*-vanilin in methanol. The Schiff base ligand (H_2L) on reaction with $Cd(NO_3)_2 \cdot 4H_2O$ and sodium azide in 1: 2: 1 ratio resulted in a tetra-nuclear complex, **1** (Scheme 1). On the other hand, when we used deprotonated isophthalic acid instead of sodium azide, we got polynuclear complex **2**. The phase purity of synthesized complexes has been checked by comparing the experimental PXRD pattern of the bulk products with the simulated XRD pattern from single crystal X-ray diffraction (Fig. S1, ESI).

IR spectra of complexes

View Article Online
DOI: 10.1039/D0NJ03325A

Besides elemental analyses, both complexes were initially characterized by the IR spectra. A strong and sharp band due to the azomethine $\nu(\text{C}=\text{N})$ group of the Schiff base appears at around 1635 cm^{-1} for both of the complexes **1** and **2**.⁴³ Complexes **1** and **2** exhibit a bands around 3170 cm^{-1} confirming the presence of the N–H group.⁴³ The presence of azido and nitrate anion in complex **1** is confirmed by the appearance of strong and sharp peaks at 2060 cm^{-1} and 1384 cm^{-1} respectively.⁴⁴ Two sharp peaks at 1557 and 1387 cm^{-1} appear for the asymmetric and symmetric stretching of $-\text{COO}^-$, respectively, for complex **2**.⁴⁵

Description of the structures

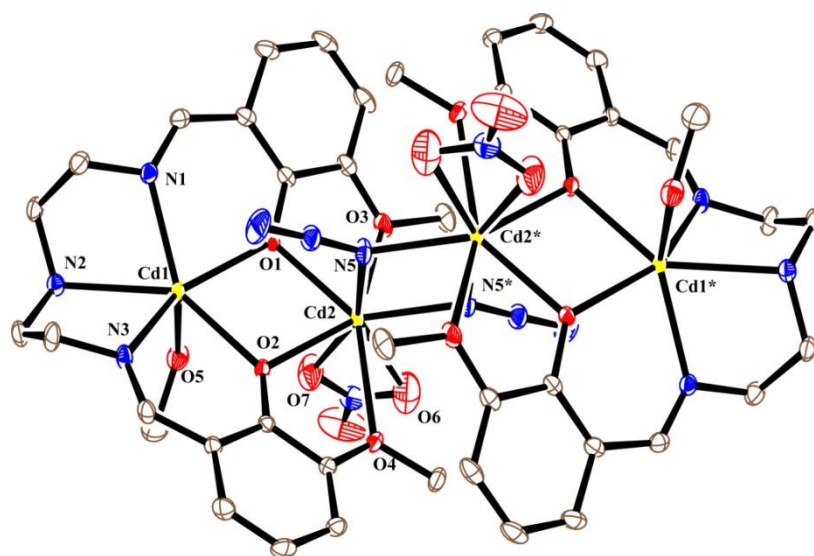


Fig. 1 ORTEP diagram of complex **1** with 20% ellipsoid probability. Hydrogen atoms are not shown for clarity.

The structure of complex **1** is shown in Fig. 1. It is a centro-symmetric discrete tetra-nuclear complex, in which two dinuclear units are bridged by two $\mu_{1,1}$ - azide co-anions. The asymmetric unit of complex **1** contains one Schiff base ligand, two Cd(II) ions, one methanol molecule, one azide and one nitrate co-anions. Cd1 centre is hexa-coordinated and Cd2 centre is octa-coordinated. Cd1 centre is coordinated by five donor atoms N1, N2, N3, O1, O2 from ligand L²⁻ and O5 from a methanol molecule. Cd2 centre is coordinated by four oxygen atoms O1, O2, O3, O4 from the ligand L²⁻, O6, O7 from the nitrate co-anion and N5, N5* from the symmetry related(1-x,1-y,1-z) azide co-anion. The Cd(II)–N(amine) distance is $2.508(3)\text{ \AA}$ whereas Cd(II)–N(imine) distances are $2.65(3)$ and $2.289(3)\text{ \AA}$. The Cd(II)–O(phenoxo)

distances are shorter at 2.266(2) and 2.305(3) Å than Cd(II)–O(methoxo) distances at 2.459(3) and 2.518(3) Å. All these distances are very similar to those observed for other structurally characterized Cd(II) complexes of this ligand.^{46,47} The Cd(II)–O(nitrate) distances are 2.419(5) and 2.767(7) Å. Selected bond lengths and bond angles of complex **1** are given in Table S1, ESI. The hydrogen atom, H5 attached to oxygen atom, O5, forms hydrogen bond with the nitrate oxygen atom (O7), details of which are given in Table S3, ESI.

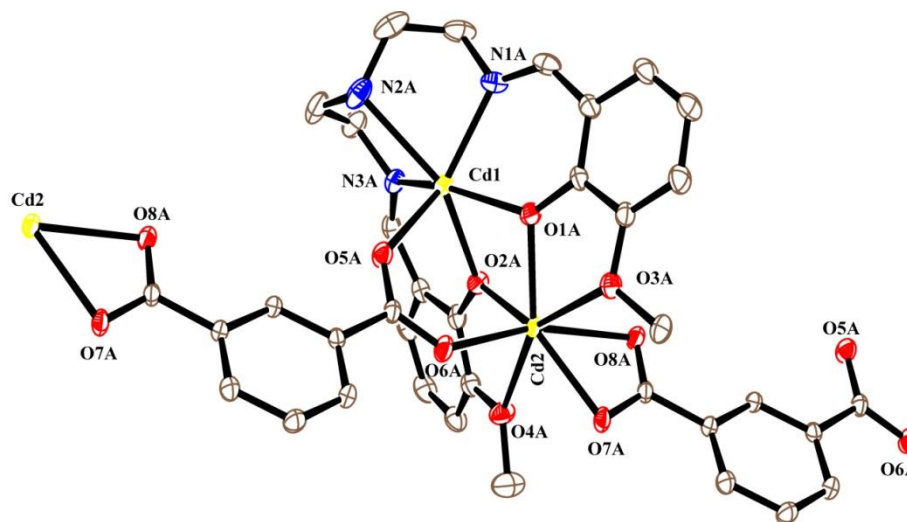


Fig. 2 ORTEP diagram of complex **2(A)** with 20% ellipsoid probability. Hydrogen atoms are not shown for clarity.

In complex **2**, there are two dinuclear units (A and B) in the asymmetric unit having equivalent structure with slight difference in bond angles and bond lengths. Each unit is a part of a polymeric chain structure formed by linking the dinuclear units by bridging isophthalate (IPA) co-ligand. A perspective view of molecule A together with the atom numbering scheme is shown in Fig. 2 and that of B is shown in Fig. S2, ESI. The Cd1 centre is hexa-coordinated being bonded by three nitrogen and three oxygen atoms, N1A, N2A, N3A, O1A, O2A from the ligand L²⁻ and O5A from isophthalate co-ligand. The Cd2 centre is hepta-coordinated being bonded by seven oxygen atoms, O1A, O2A, O3A, O4A from the ligand and O6A, O7A, O8A from isophthalate co-ligand. The Cd(II)–O(phenoxo) bond lengths are within the range of 2.227(3)–2.303(3) Å. The Cd(II)–N(amine) bond lengths are 2.520(3) and 2.467(5) Å, whereas the Cd(II)–N(imine), Cd(II)–O(methoxo) and Cd(II)–O(carboxylate) bond lengths are in the range of 2.285(6)–2.315(6) Å, 2.569(4)–2.700(5) Å and

2.210(4)–2.309(4) Å, respectively. Selected bond lengths and bond angles of complex **2** are given in Table S2, ESI. In this complex, the deprotonated isophthalic acid bridges three Cd(II) centres *via* ($1\kappa^2\text{O},\text{O}':2\kappa\text{O},\text{O}'$) mode where both oxygen atoms of one carboxylate bridges two Cd(II) centres of one dinuclear unit, while the other carboxylate bridges the Cd(II) centre of a symmetry related dinuclear unit. Thus, each IPA acts as a μ_3 -bridging ligand to form the polymeric chain (Fig. 3). The hydrogen atom, H2AA, attached to nitrogen atom, N2B, forms intramolecular hydrogen bonding interaction with the oxygen atom, O9 of solvent methanol molecule and the hydrogen atom H3AA, attached to the O9, forms hydrogen bonding interaction with the carboxylate anion oxygen atom O5B. The H-bonding parameters are given in Table S3, ESI.

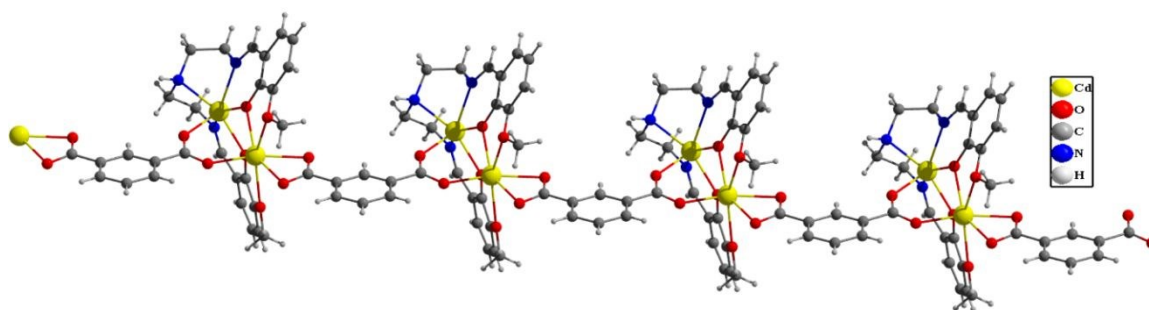


Fig. 3 Polymeric chain of complex **2** built by units A. A closely comparable chain is formed by units B.

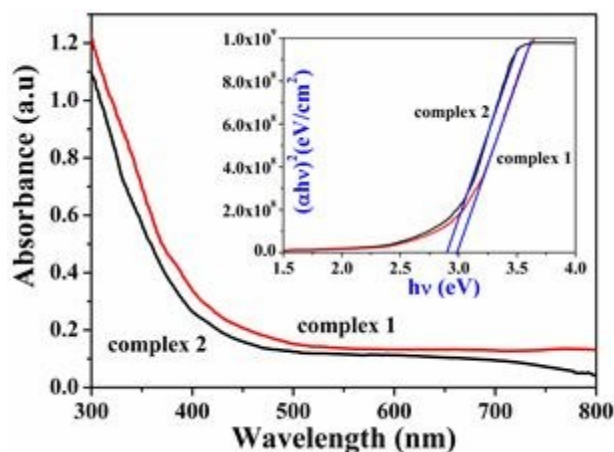


Fig. 4 UV-Vis spectra (thin film) of complexes **1** and **2**, inset: band gap

Optical study

Fig. 4 shows the UV-Vis absorption spectra of both complexes **1** and **2** (thin films). The band gap energy was evaluated from the absorption spectra using the following relation:

$$(\alpha h\nu) \propto (h\nu - E_g)^n \quad (1)$$

Where, E_g is the energy band gap, α is the absorption coefficient, n is a coefficient having the value $\frac{1}{2}$ for allowed direct band-to-band transition. The Tauc plot $(\alpha h\nu)^2$ vs. $(h\nu)$ is shown as the inset of Fig. 4. Optical band gap was calculated from this relation by plotting $(\alpha h\nu)^2$ versus $h\nu$ and extrapolating the linear portion of the curve to the x-axis; α being the absorption coefficient and $h\nu$, the photon energy. The band gap (E_g) was calculated to be 2.98 and 2.90 eV for complexes **1** and **2**, respectively. Wide band gap of this material is a good signature for opto-electronic properties. Slight decrease of band gap for complex **2** may be due to its polymeric nature.⁴⁸ Complex **2** ensures surface modification by lowering band width (d) of valence band (V_B) and conduction band (C_B). As a result, number of excitons in VB and CB increases and it leads to lowering of band gap energy. The absorption spectra of complexes **1** and **2** (in methanol solution) are given in supporting information (Fig. S3, ESI). Both complexes show a sharp rise in absorption from 400 nm and maximum absorption occurs in the UV region at 350 nm due to $n-\pi^*$ transition.³⁹

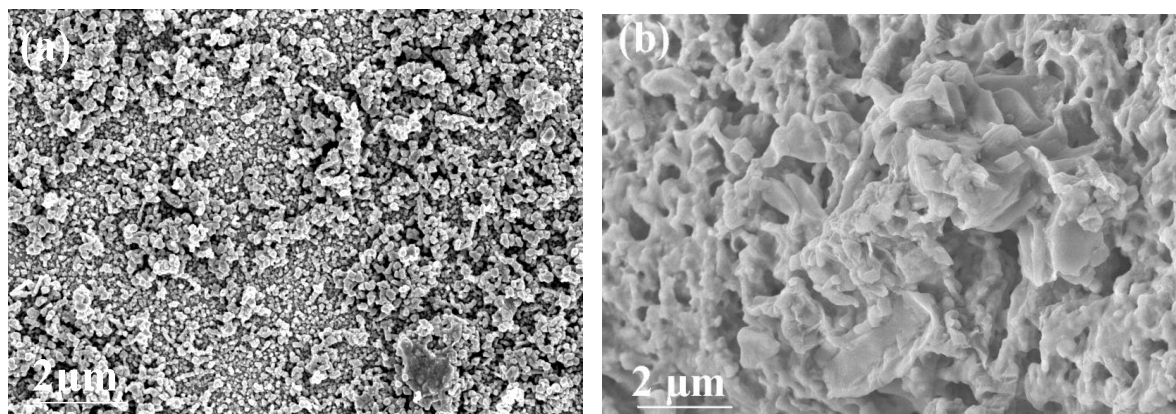


Fig. 5 (a) Thin film FESEM images of complex **1** and (b) complex **2**.

Morphological analysis of thin films

Fig. 5 (a) represents FESEM image of complex **1**. It shows granular morphology along with randomly oriented agglomerated particles. Average grain size of discrete particle has been estimated to be 50-55 nm. However, agglomerated particles form their own moiety make overall morphology “uneven”. FESEM image of complex **2** is represented in Fig. 5b. It shows highly porous fleshy structure in combination with islands and coarse wells. Each island is composed with uniformly distributed spherical grains. The wells and islands are distinct but the grains are invisible due to formation of islands which increases the surface to a large extent. These wells can be regarded as trapped zones for electrons.⁴⁹ Now applying a fixed potential/frequency stimulates the trapped electrons and electrons get released from trapped zones and shows current amplification (photoexcitation).

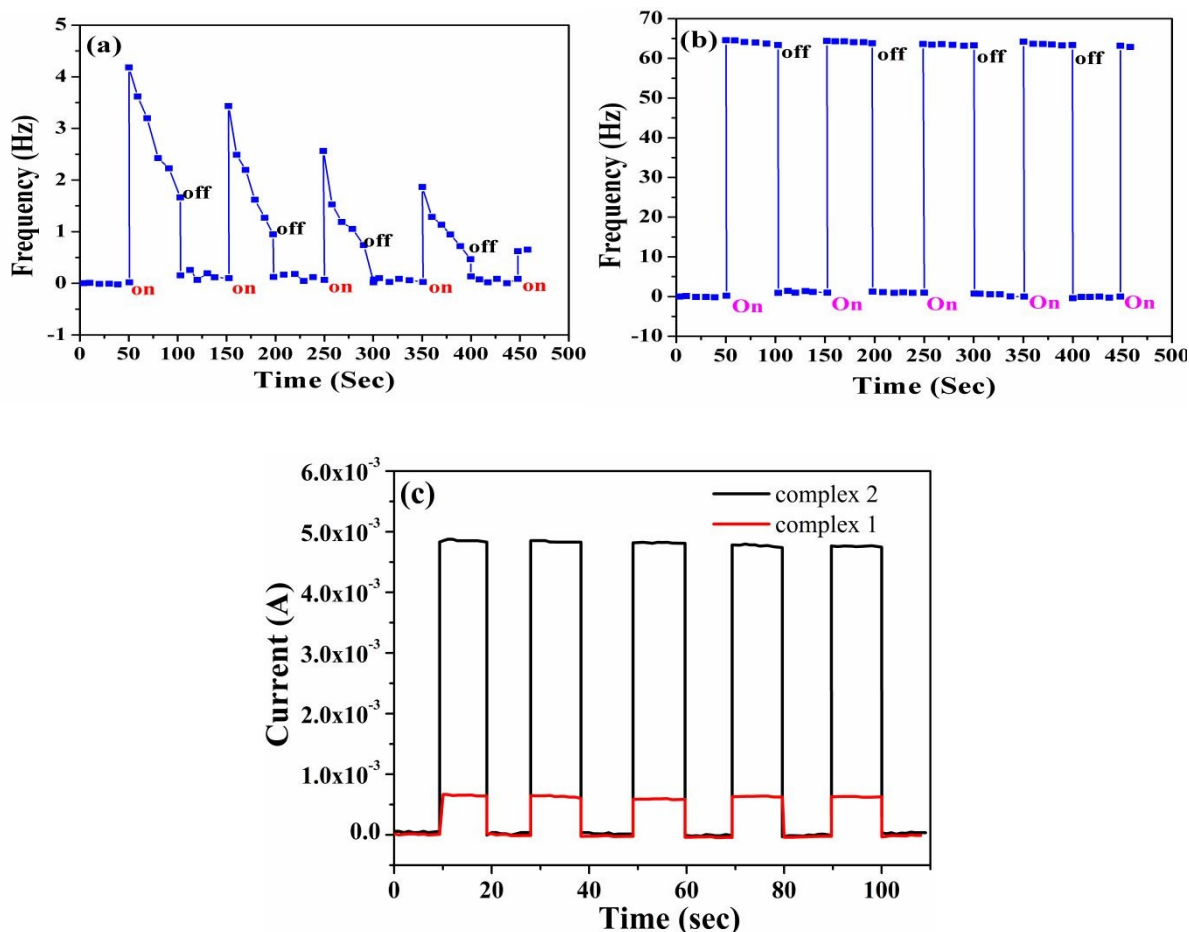


Fig. 6 Photocurrent responses of (a) complex **1** and (b) complex **2** (c) Photocurrent versus time (I–t) plots of complexes **1** and **2**.

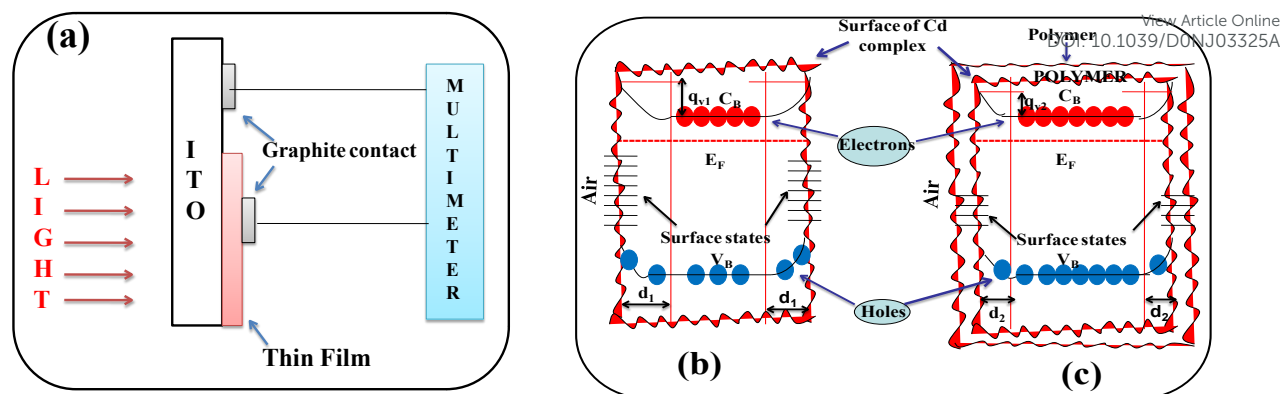


Fig. 7 (a) Schematic of frequency switching study (b) Band diagram of complex 1 and (c) complex 2.

Frequency switching:

To measure the switching behaviour of synthesized materials, light dependent exciton generation was studied where top and bottom contacts were made from deposited material and ITO layer using colloidal silver paste. An external light source of intensity 1 Sun was used to fall on the ITO so that it could pass the film. From the response ratio curve (Fig. 6b), it could be observed that as soon as the light hit the material the frequency increased to ~ 65 Hz and became steady for 50 seconds. This frequency is oscillation frequency and it goes to 'zero' as soon as light is chocked. Switching off the light allowed the excitons to be at ground state and resulted in their fast recombination; hence, no pulse/frequency was generated at this stage. Repeatability of this experiment was viewed for more than 30 cycles indicating steady nature of the polymer material. Same arrangement was repeated for complex 1 but no significant response was detected (Fig. 6a). The transient photocurrent with respect to time was measured under light illumination of 100 mW cm^{-2} at 1 V, which is shown in Fig. 6c. To compare the photosensitivity (A/W) of each device individual dark currents were subtracted from light currents. It has been observed that the device fabricated with complex 1 showed photosensitivity 1.18. Whereas, the device made from complex 2 showed a high photosensitivity 5.41. These photosensitivity values are consistent with the data obtained from I-V measurement (Table 2). In general photoresponse is a speedy electron transfer process where photoexcited electrons are transferred from the highest occupied molecular orbital (HOMO) to the lowest unoccupied molecular orbital (LUMO). High photosensitivity of complex 2 indicates efficient photogenerated electron-hole separation and retardation of recombination process. The phenomenon could also be explained by introducing surface state

energy concept observed in polymer complexes.⁴⁹ Polymer encapsulation causes surface modification of the material and lowers down the width (d) of the depletion region (Fig. 7(c)). As a result, the number of separated electron-hole pairs (excitons) in between VB and CB increases which leads to increase in exciton related emission by reducing recombination process.⁴⁹ The increased number of excitons results high frequency switching behavior for complex 2 and suggest that the complex can be a promising candidate for photo switch. Fig. 7(b) shows the band energy diagram of complex 1 where no such surface modification occurs.

Electrical Characterization: I-V measurement

Two-probe I-V measurement was carried out under dark and light illumination (1 Sun) condition from potential -1 to $+1$ V taking Al as metal contact. Fig. 8 (a) shows I-V nature for complex 1. Nonlinear nature of I-V curve shows good rectifying behaviour which is an indication of Schottky barrier diode (SBD). The non-linear I-V characteristic also indicates formation of depletion region in between the interface. In forward bias thin films of both complexes (complexes 1 and 2) show enhanced rectifying behaviour under illumination. In case of complex 2, the ratio of on/off was calculated to be 2.37 and 12.84 under dark and light illumination, respectively (Table 2). It indicates high rectifying property of the diode which is comparable to the others of same type.^{35,50-52} Room temperature conductivities of complexes 1 and 2 were evaluated from I-V curves. It has been observed that for both complexes light illumination results in increase of conductivity compared to dark condition (Tables 3 and 4). Generally thin film faces intrinsic defects by atmospheric oxygen or gas molecules, which lead to band bending from its bulk counterpart and thereby affect on electronic transition. The defects become high at the grain boundaries of the nanoparticles and causes trapping of electrons. By applying certain bias, these trapped zones become saturated and electrons get free. Therefore, an enhanced current density is observed in forward bias. In reverse bias, opposite phenomenon is found to be happened. Reversing the bias decreases the electrostatic attraction of trapped zones and results increase in an leakage current density. The current generated in the reverse bias comes from the loss of junction properties by free minority carriers which in turn raise the reverse saturation current. For both complexes a detail SBD related parameter like photosensitivity, conductivity, ideality factor, diffusion coefficient, effective mobility etc. were calculated (Table 3 and 4). The better semiconducting feature of the polymeric complex 2 can be attributed to the charge

delocalization throughout the polymeric chain *via* highly π conjugated dicarboxylic acid linkers. Further, the supramolecular interactions through closely spaced polymeric chains can also improve the semiconducting property of complex **2** as charge can move through non-covalent supramolecular contacts (e.g. C–H... π , π ... π) *via* “hopping transport” phenomenon.⁵³ But in case of complex **1**, which is a discrete species and charge may move only through noncovalent supramolecular contacts (e.g. C–H... π , π ... π) *via* “hopping transport” phenomenon” giving rise to weak semiconducting ability.

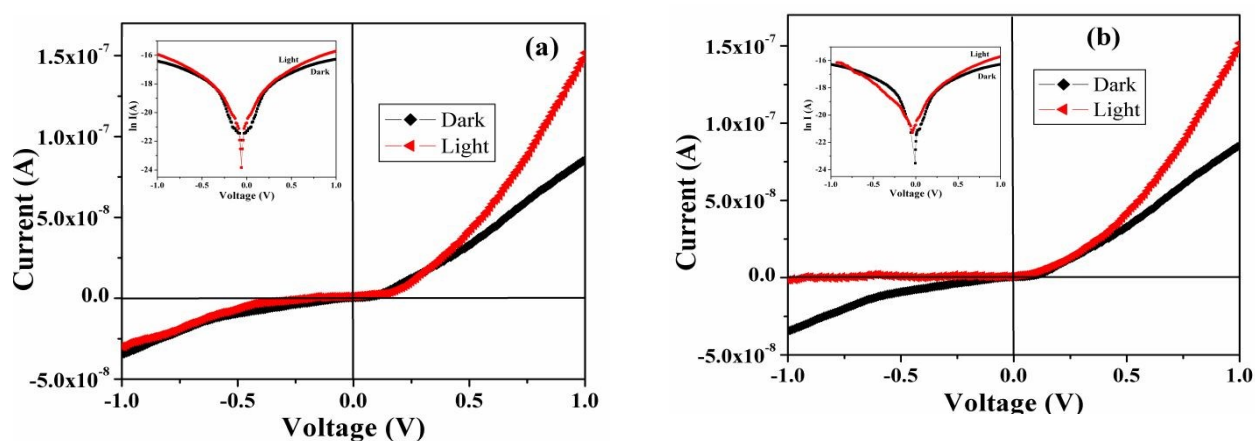


Fig. 8 I–V characteristic curve of (a) ITO/complex **1**/Ag thin film and (b) ITO/ complex **2**/Ag thin film.

Electrical characterization and photosensitivity

The current voltage characteristics of complexes **1** and **2** based devices are shown in Fig. 8. It exhibits a highly non-linear rectifying Schottky diode behaviour. The non-linearity of the I–V curve indicates non-ohmic nature which is highly influenced by incident radiation. Complex **2** shows linearity of current axis at low reverse bias but at higher bias due to high series resistance current no longer becomes linear. The rectification ratios under dark and photo illumination have been calculated to be 3 and 6, respectively for complex **1** and 2.51 and 17 respectively for complex **2**. Thus, an enhanced rectification in presence of light is obvious for complex **2**. To understand the charge transport mechanism, thermoionic emission theory was introduced to analyze the I–V curve using Cheung standard equation for Schottky diodes.⁵⁴

$$I = I_0 \left[\exp\left(\frac{qV}{\eta kT}\right) - 1 \right] \quad (2)$$

where I ; forward current, I_0 ; saturation current (reverse), V ; applied potential, q ; electronic charge, k ; Boltzmann constant, T ; absolute temperature, η ; ideality factor.

The intercept of $\ln(I)$ where $V = 0$ gives I_0 from the following equation

$$I_0 = AA^* T^2 \exp\left(\frac{-q\Phi_B}{KT}\right) \quad (3)$$

Here, A stands for diode area, Φ_B represents barrier potential height and A^* is the Richardson constant. For all the measurements effective diode area was $7.065 \times 10^{-2} \text{ cm}^2$ and the value of Richardson constant was considered as $32 \text{ A K}^{-2} \text{ cm}^{-2}$.

To determine other device parameters, following equations were used.⁵⁵

$$\frac{dv}{d\ln I} = \frac{\eta kT}{q} + IR_s \quad (4)$$

Series resistance (R_s) was calculated from the following equations (5 and 6).

$$H(I) = V - \left(\frac{\eta kT}{q}\right) \ln\left(\frac{I}{AA^* T^2}\right) \quad (5)$$

$$H(I) = IR_s + \eta\Phi_B \quad (6)$$

Equation (4) represents straight line and indicates downward-curvature region of the forward bias where R_s predominates. Thus, from the slope of $dV/d\ln I$ vs. I (Fig. 9a and 9b) R_s is calculated and intercept of the same plot at y axis gives ideality factor (η). The η values under dark and illumination were calculated to be 2.58 and 1.46 for complex **1** and 2.5 and 1.24 for complex **2**, respectively. Analyzing η values, it can be concluded that the MS junction of complex **2** is less deviate from ideality. Hence complex **2** is more suitable for device fabrication. This deviation comes from in-homogeneities in barrier height (Φ_B), mismatch of interfacial states and series resistance in the junction.⁵⁶ Using the measured η value, H was calculated from equation (5). Plot of $H(I)$ vs. I also represents a straight line whose intercept at y -axis becomes equal to $\eta\Phi_B$ (Fig. 10). The measured barrier height (Φ_B), ideality factor (η) and series resistance (R_s) under the dark and illumination etc. for the MS junction of complex **1** and complex **2** are separately enlisted in Table 3 and 4. From the Tables it is clear that the series resistance (R_s) for both complexes obtained from two different methods using Cheung's functions are in concurrence with each other.

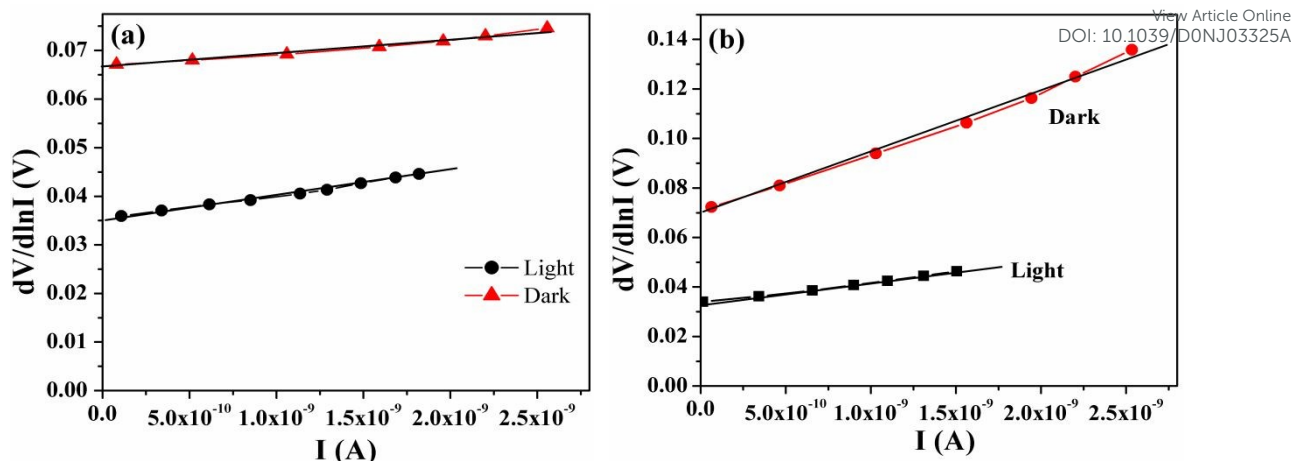


Fig. 9 $dV/d\ln I$ vs. I plot under dark and illumination conditions for (a) complex 1 and (b) complex 2.

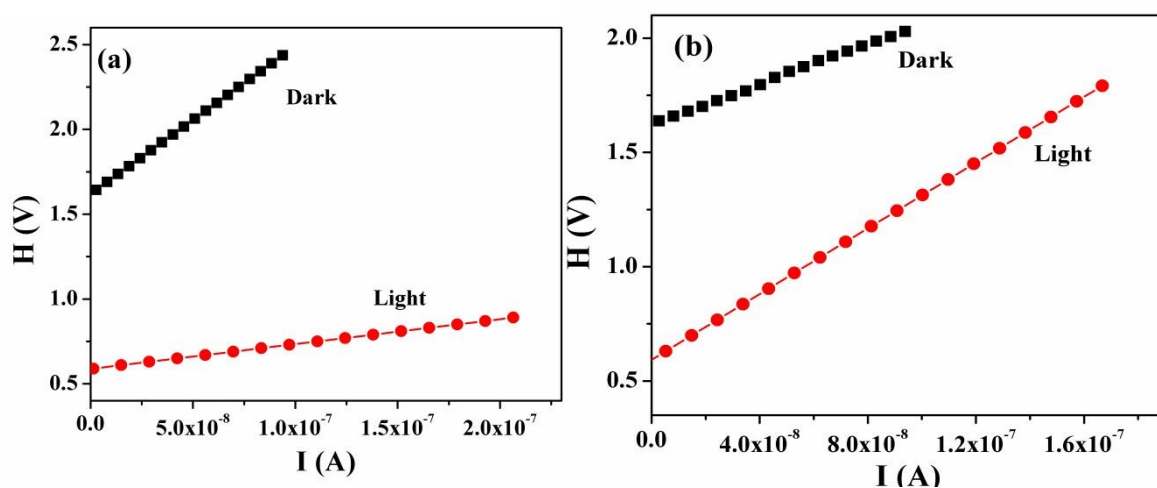


Fig. 10 $H(I)$ vs I graph under dark and illumination condition for (a) complex 1 and (b) complex 2 thin film devices, respectively.

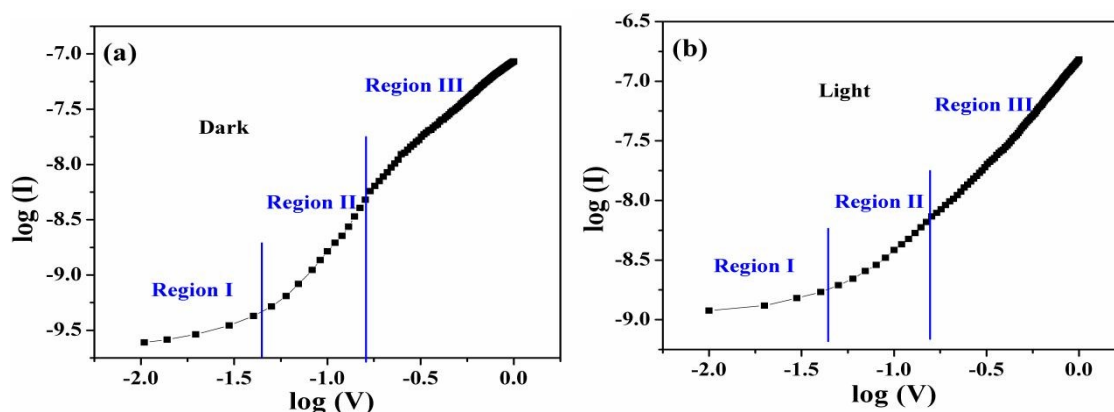


Fig. 11 Plot of $\log(I)$ versus $\log(V)$ for complex 2 under (a) dark and (b) illumination.

To gain better perceptiveness of the MS junction, consideration of interface carrier transport is useful. Fig. 11 represents the log-log (I-V) plot of complex **2**. It implies existence of different conduction regions. We can segregate it into three distinct linear regions considering different slopes. Each partition has unique features corresponding to electron transportation. Presence of interfacial deep wells at M-S junction is responsible for alteration of the slopes which in turn alters the carrier concentration of individual partition. At low bias i.e. region-I, current increases proportionally with voltage, confirming the ohmic nature of the device. Therefore, region-I is attributed to thermionic emission where current is controlled by the bulk electrons of the material, rather than the injected free carriers.⁵⁷⁻⁵⁹ After that, I-V curve proceeds smoothly and follows power law ($I \propto V^n$), which is assigned as region II. In this region, the current is governed by space charge limit current (SCLC) where current becomes directly proportional to the square of the applied potential ($I \propto V^2$).^{60,61} Due to thermionic oscillation injected carriers become highly activated and started to spread by creating a space charge region in conduction path. Just behind the region (II), current becomes more steeper and at further higher bias, the current increases sharply because of excessive electron accumulation which triggers to exceed the 'trap-filled' limit of the diode easily.⁵⁷ So, it can be concluded that region I is devoted for charge transportation and regions II and III can be categorised as SCLC and trap free SCLC at their respective forward bias. To understand the charge transport mechanism precisely, region II has been selected to apply SCLC on it. Effective carrier mobility at region II is measured from the slope of I vs V^2 (Fig. 12) by using the Mott-Gurney equation⁶²

$$J = \frac{9}{8} \mu_{\text{eff}} \epsilon_0 \epsilon_r \left(\frac{V^2}{d^3} \right) \quad (7)$$

where J , ϵ_0 and ϵ_r represent current density, vacuum permittivity dielectric constant, respectively. The effective carrier mobility (μ_{eff}) was calculated to $1.49 \times 10^{-8} \text{ cm}^2 \text{ V}^{-1} \text{ s}^{-1}$, which is at par for the compounds. Dielectric constant (DC) was measured under constant bias at saturation capacitance from capacitance vs frequency plot. The variation of the capacitance (c) as a function of the frequency (f) at constant bias potential was shown in Fig. S4, ESI. The room temperature capacitance of the complex is found to be frequency dependent at relatively lower frequencies. The capacitance decreases with increasing frequency and becomes saturated at higher frequency and the saturation capacitance is found to be $20 \times 10^{-12} \text{ F}$. The following conventional equation is used to measure dielectric constant.⁶³

$$\epsilon_r = \frac{1}{\epsilon_0} \cdot \frac{C \cdot L}{A} \quad (8)$$

View Article Online
DOI: 10.1039/D0NJ03325A

Where, ϵ_0 is the permittivity of free space, ϵ_r is the relative permittivity of the complex, C is the capacitance (at saturation) and L is the thickness and A is effective area of the film. By using capacitance value (saturation) the DC comes out to be 5.674. Other device parameters such as carrier concentration (N), carrier lifetime (τ) and diffusion length (L_D) were estimated using the following set of equations.⁶⁴

$$N = \frac{\sigma}{q\mu_{eff}} \quad (9)$$

$$\tau = \frac{9\epsilon_0\epsilon_r A}{8d} \left(\frac{V}{I}\right) \quad (10)$$

$$L_D = \sqrt{2D\tau} \quad (11)$$

Activity of any SBD can be judged by its diffusion length (L_D). High value of L_D ensures better device performance.

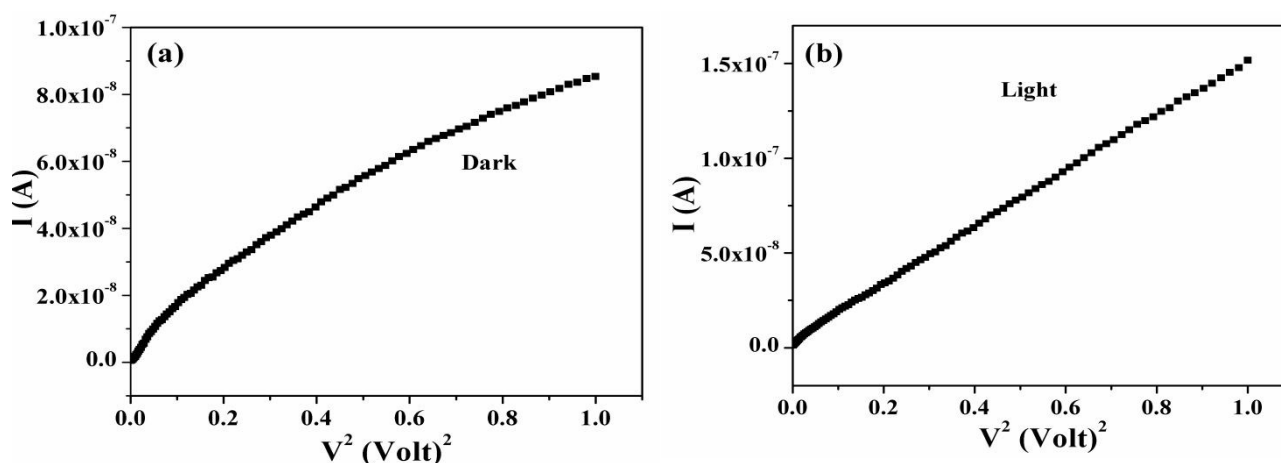


Fig. 12 I vs V^2 plot for complex 2 device in (a) dark and (b) illumination

From the slope of log I vs log plot of region II (Fig. 11) carrier lifetime (τ) was calculated. It has been found that for complex 2 carrier life time is shorter in comparison to complex 1. It is a good signature for device fabrication with complex 2. Diffusion coefficient was measured following Einstein–Smoluchowski equation.^{65,66}

$$\mu_{ef} = \frac{qD}{kT} \quad (12)$$

The obtained values of the diode and transport parameters are listed in Table 3 and Table 4 for complexes 1 and 2, respectively.

Conclusion

View Article Online
DOI: 10.1039/D0NJ03325A

We have reacted the flexidentate ligand, *N,N'*-bis(3-methoxysalicylidene)diethylenetriamine (H_2L), with cadmium nitrate in presence of bridging co-anions, azide or isophthalate. The azide ion yields a discrete tetra-nuclear complex whereas a one-dimensional polymeric complex is produced with bridging isophthalate. We have explored the effect of this structural variation on the optoelectrical properties of the synthesized complexes. Interestingly, it has been found that only polymeric complex **2** shows considerable photo switching phenomenon. In complex **2** mobilization of charge carriers takes place *via* highly π conjugated organic linkers and the 1D CP ensures surface modification which in turn increases the number of excitons in between VB and CB. The result is the substantial reduction of recombination process and therefore material shows enhanced current intensity under the irradiance of light. Moreover, the fabricated devices using complexes **1** and **2** exhibit a non-linear rectifying behavior under dark and illumination conditions at the applied potential of ± 1.0 V. Several device parameters have been measured and the charge transport properties have been analyzed on the basis of the Schottky diode mechanism. The estimated mobility, lifetime, carrier diffusion length, ideality factor clearly show that the device performance of the polymeric complex is much better compared to the discrete complex and it would be a promising material for light sensing electronic devices as well as for diode fabrication.

Supporting Information

CCDC 1975601–1975602 contain the supplementary crystallographic data for this paper. These data can be obtained free of charge from The Cambridge Crystallographic Data Centre via www.ccdc.cam.ac.uk/data_request/cif. bond lengths and angles of complexes **1** and **2**, PXRD pattern of complexes **1** and **2**, UV-Vis spectra of complexes **1** and **2** in methanol solution, ORTEP of complex **2B**, Capacitance *vs.* Frequency plot, Dielectric *vs.* Frequency plot for complex **2**.

Acknowledgement

T. K. G. is thankful to the University Grants Commission (UGC), New Delhi, for Senior Research Fellowship [Sr. no. 2061510191, Ref. no. 21/06/2015 (I) EU-V, dated 15/12/2015]. Sumanta Jana acknowledges UGC India for offering him Dr. D. S. Kothari Postdoctoral Fellowship [Award letter no. F.4-2/2006 (BSR)/CH/18-19/0017]. We thank USIC, The

University of Burdwan, West Bengal, India, for providing the single crystal X-ray diffractometer facility.

References

- (1) L. K. Das and A. Ghosh, *CrystEngComm*, 2013, **15**, 9444–9456.
- (2) D. Nagaraju, D. G. Bhagat, R. Banerjee and U. K. Kharul, *J. Mater. Chem. A*, 2013, **1**, 8828–8835.
- (3) D. K. Maity, A. Dey, S. Ghosh, A. Halder, P. P. Ray and D. Ghoshal, *Inorg. Chem.*, 2018, **57**, 251–263.
- (4) R. Haldar, S. K. Reddy, V. M. Suresh, S. Mohapatra, S. Balasubramanian and T. K. Maji, *Chem. Eur. J.* 2014, **20**, 4347–4356.
- (5) H. Furukawa, K. E. Cordova, M. O’Keeffe and O. M. Yaghi, *Science*, 2013, **341**, 1230444.
- (6) Y. He, B. Li, M. O’Keeffe and B. Chen, *Chem. Soc. Rev.*, 2014, **43**, 5618–5656.
- (7) C. Janiak and J. K. Vieth, *New J. Chem.*, 2010, **34**, 2366–2388.
- (8) Y. Yang, F. Wang, Q. Yang, Y. Hu, H. Yan, Y.-Z. Chen, H. Liu, G. Zhang, J. Lu, H.-L. Jiang and H. Xu, *ACS Appl. Mater. Interfaces*, 2014, **6**, 18163–18171.
- (9) B. Gole, U. Sanyal and P. S. Mukherjee, *Chem. Commun.*, 2015, **51**, 4872–4875.
- (10) L.-W. Zeng, K.-Q. Hu, L. Mei, F.-Z. Li, Z.-W. Huang, S.-W. An, Z.-F. Chai and W.-Q. Shi, *Inorg. Chem.*, 2019, **58**, 14075–14084.
- (11) H. Li, Y. Wang, Y. He, Z. Xu, X. Zhao and Y. Han, *New J. Chem.*, 2017, **41**, 1046–1056.
- (12) K. M. L. Taylor-Pashow, J. D. Rocca, Z. Xie, S. Tran and W. Lin, *J. Am. Chem. Soc.*, 2009, **131**, 14261–14263.
- (13) H. Kitagawa, *Nature Chemistry*, 2009, **1**, 689–690.

- 1
2
3
4
5
6
7
8
9
10
11
12
13
14
15
16
17
18
19
20
21
22
23
24
25
26
27
28
29
30
31
32
33
34
35
36
37
38
39
40
41
42
43
44
45
46
47
48
49
50
51
52
53
54
55
56
57
58
59
60
- (14) M. Inukai, S. Horike, T. Itakura, R. Shinozaki, N. Ogiwara, D. Umeyama, S. Nagakai, Y. Nishiyama, M. Malon, A. Hayashi, T. Ohhara, R. Kiyanagi and S. Kitagawa, *J. Am. Chem. Soc.*, 2016, **138**, 8505–8511. View Article Online
DOI: 10.1039/C6NJ03325A
- (15) S. Ghosh, Y. Ida, T. Ishida and A. Ghosh, *Cryst. Growth Des.*, 2014, **14**, 2588–2598.
- (16) P. Ghorai, A. Dey, P. Brandão, J. Ortega-Castro, A. Bauza, A. Frontera, P. P. Ray and A. Saha, *Dalton Trans.*, 2017, **46**, 13531–13543.
- (17) R. Matsuoka, R. Toyoda, R. Sakamoto, M. Tsuchiya, K. Hoshiko, T. Nagayama, Y. Nonoguchi, K. Sugimoto, E. Nishibori, T. Kawai and H. Nishihara, *Chem. Sci.*, 2015, **6**, 2853–2858.
- (18) P. Kar, R. Haldar, C. J. Gómez-García and A. Ghosh, *Inorg. Chem.*, 2012, **51**, 4265–4273.
- (19) L. K. Das, C. Diaz and A. Ghosh, *Cryst. Growth Des.*, 2015, **15**, 3939–3949.
- (20) S. Ganguly, P. Kar, M. Chakraborty and A. Ghosh, *New J. Chem.*, 2018, **42**, 9517–39529.
- (21) L. K. Das, C. J. Gómez-García and A. Ghosh, *Dalton Trans.*, 2015, **44**, 1292–1302.
- (22) I.-H. Park, R. Medishetty, J.-Y. Kim, S. S. Lee and J. J. Vittal, *Angew. Chem. Int. Ed.*, 2014, **53**, 5591–5595.
- (23) S. Jana and S. Chattopadhyay, *Polyhedron*, 2014, **81**, 298–307.
- (24) Q. Zha, X. Rui, T. Wei and Y. Xie, *CrystEngComm*, 2014, **16**, 7371–7384.
- (25) S. Ghosh, G. Aromí, P. Gamez and A. Ghosh, *Eur. J. Inorg. Chem.*, 2015, 3028–3037.
- (26) R. Haldar and T. K. Maji, *CrystEngComm*, 2013, **15**, 9276–9295.
- (27) N. Stock and S. Biswas, *Chem. Rev.*, 2012, **112**, 933–969.
- (28) S. Khan, S. Halder, P. P. Ray, S. Herrero, R. González-Prieto, M. G. B. Drew and S. Chattopadhyay, *Cryst. Growth Des.*, 2018, **18**, 651–659.
- (29) L. Sun, M. G. Campbell and M. Dincă, *Angew. Chem. Int. Ed.*, 2016, **55**, 3566–3579.

- (30) R. Kaur, K.-H. Kim, A. K. Paul and A. Deep, *J. Mater. Chem. A*, 2016, **4**, 3991–4002. View Article Online
DOI: 10.1039/D0NJ03325A
- (31) K. Naskar, A. Dey, B. Dutta, F. Ahmed, C. Sen, M. H. Mir, P. P. Roy and C. Sinha, *Cryst. Growth Des.*, 2017, **17**, 3267–3276.
- (32) C. A. Kent, D. Liu, T. J. Meyer and W. Lin, *J. Am. Chem. Soc.*, 2012, **134**, 3991–3994.
- (33) A. Dey, S. Middya, R. Jana, M. Das, J. Datta, A. Layek and P. P. Ray, *J. Mater. Sci.: Mater. Electron.*, 2016, **27**, 6325–6335.
- (34) J. Zhu, W. A. Maza and A. J. Morris, *J. Photochem. Photobiol.*, 2017, **344**, 64–77.
- (35) S. Roy, A. Dey, P. P. Ray, J. Ortega-Castro, A. Frontera and S. Chattopadhyay, *Chem. Commun.*, 2015, **51**, 12974–12976.
- (36) B. Dutta, R. Jana, A. K. Bhanja, P. P. Ray, C. Sinha and M. H. Mir, *Inorg. Chem.*, 2019, **58**, 2686–2694.
- (37) S. Dutta, S. Chakraborty, M. G. B. Drew, A. Frontera and A. Ghosh, *Cryst. Growth Des.*, 2019, **19**, 5819–5828.
- (38) T. K. Ghosh, P. Mahapatra, S. Jana and A. Ghosh, *CrystEngComm*, 2019, **21**, 4620–4631.
- (39) T. K. Ghosh, S. Jana and A. Ghosh, *Inorg. Chem.*, 2018, **57**, 15216–15228.
- (40) G. M. Sheldrick, *Acta Cryst.*, 2015, **C71**, 3–8.
- (41) O.V. Dolomanov, L. J. Bourhis, R. J. Gildea, J. A. K. Howard and H. Puschmann, Olex2: A complete structure solution, refinement and analysis program, *J. Appl. Cryst.*, **42**, 2009, 339–341.
- (42) SAINT and SADABS, version 6.02 and version 2.03; Bruker AXS, Inc.: Madison, WI, 2002.
- (43) T. K. Ghosh, P. Mahapatra, M. G. B. Drew, A. Franconetti, A. Frontera and A. Ghosh, *Chem. Eur. J.*, 2020, **26**, 1612–1623.
- (44) A. Das, S. Jana and A. Ghosh, *Cryst. Growth Des.*, 2018, **18**, 2335–2348.
- (45) C. C. R. Sutton, G. D. Silva and G. V. Franks, *Chem. Eur. J.*, 2015, **21**, 6801–6805.
- (46) B. Naskar, R. Modak, D. K. Maiti, M. G. B. Drew, A. Bauza, A. Frontera, C. Das Mukhopadhyay, S. Mishra, K. D. Saha and S. Goswami, *Dalton Trans.*, 2017 **46**, 9498–9510.
- (47) J. Chakraborty, S. Thakurta, B. Samanta, A. Ray, G. Pilet, S. R. Batten, P. Jensen and S. Mitra, *Polyhedron*, 2007, **26**, 5139–5149.
- (48) K. W. Liu, R. Chen, G. Z. Xing, T. Wu and H. D. Sun, *Appl. Phys. Lett.*, 2010, **96**, 023111.

- (49) S. Jana, B. C. Mitra, P. Bera, M. Sikdar and A. Mondal, *J. Alloy. Compd.*, 2014, **602**, 42–48. Article Online
DOI: 10.1039/C4NJ03325A
- (50) B. Dutta, A. Dey, K. Naskar, S. Maity, F. Ahmed, S. Islam, C. Sinha, P. Ghosh, P. P. Ray and M. H. Mir, *New J. Chem.*, 2018, **42**, 10309–10316.
- (51) B. Dutta, R. Jana, C. Sinha, P. P. Ray and M. H. Mir, *Inorg. Chem. Front.*, 2018, **5**, 1998–2005.
- (52) S. Roy, S. Halder, M. G. B. Drew, P. P. Ray and S. Chattopadhyay, *New J. Chem.*, 2018, **42**, 6062–6076.
- (53) I. Stassen, N. Burtch, A. Talin, P. Falcaro, M. Allendorf and R. Ameloot, *Chem. Soc. Rev.*, 2017, **46**, 3185–3241.
- (54) E. H. Rhoderick and R. H. Williams, *Metal–Semiconductor Contacts*, Clarendon Press, Oxford, 2nd edn, **1988**.
- (55) S. K. Cheung and N. W. Cheung, *Appl. Phys. Lett.*, 1986, **49**, 85–87.
- (56) R. K. Gupta and F. Yakuphanoglu, *Sol. Energy*, 2012, **86**, 1539–1545.
- (57) İ. Taşçıoğlu, U. Aydemir and Ş. Altındal, *J. Appl. Phys.*, 2010, **108**, 064506.
- (58) Y. S. Ocak, M. Kulakci, T. Kılıçoğlu, R. Turan and K. Akkılıç, *Synth Met.*, 2009, **159**, 1603–1607.
- (59) R. Şahingöz, H. Kanbur, M. Voigt and C. Soykan, *Synth Met.*, 2008, **158**, 727–731.
- (60) A. Jain, P. Kumar, S. C. Jain, V. Kumar, R. Kaur and R. M. Mehra, *J. Appl. Phys.*, 2007, **102**, 094505.
- (61) Ş. Aydoğan, M. Sağlam and A. Türüt, *J. Phys. Condens. Mater* 2006, **18**, 2665–2676.
- (62) P. W. M. Blom, M. J. M. d. Jong and M. G. v. Munster, *Phys. Rev. B*, 1997, **55**, R656–R659.
- (63) A. K. Bhanja, S. Mishra, K. Naskar, S. Maity, K. Das Saha and S. Sinha, *Dalton Trans.*, 2017, **46**, 16516–16524.
- (64) S. Middy, A. Layek, A. Dey, J. Datta, M. Das, C. Banerjee and P. P. Ray, *ChemPhysLett.*, 2014, **610–611**, 39–44.
- (65) M. Das, J. Datta, A. Dey, R. Jana, A. Layek, S. Middy and P. P. Ray, *RSC Adv.*, 2015, **5**, 101582–101592.
- (66) S. Halder, M. Das, K. Ghosh, A. Dey, B. B. Show, P. P. Ray, and P. Roy, *J. Mater. Sci.*, 2016, **51**, 9394–9403.

Table 1: Crystal data and structure refinement of complexes **1** and **2**.View Article Online
DOI: 10.1039/D0NJ03325A

Complex	1	2
Chemical formula	C ₄₂ H ₅₄ Cd ₄ N ₁₄ O ₁₆	C _{28.5} H ₂₉ Cd ₂ N ₃ O _{8.5}
Formula weight	1460.63	774.35
Crystal system	Orthorhombic	Triclinic
Space group	<i>Pbca</i>	<i>P</i> $\bar{1}$
<i>a</i> (Å)	12.4732(5)	10.570(2)
<i>b</i> (Å)	17.7256(7)	17.255(4)
<i>c</i> (Å)	23.1634(10)	17.545(4)
α (°)	90	72.062(3)
β (°)	90	72.882(3)
γ (°)	90	72.850(3)
<i>V</i> (Å ³)	5121.3(4)	2835.2(11)
<i>Z</i>	4	4
ρ_{calc} (g cm ⁻³)	1.894	1.814
<i>T</i> (K)	300	296
μ (Mo K α) (mm ⁻¹)	1.721	1.558
<i>F</i> (000)	2896	1540
R(int)	0.028	0.039
Total reflections	111500	20921
Unique reflections	5264	10704
Reflections with <i>I</i> > 2 σ (<i>I</i>)	4716	8103
[<i>I</i> > 2 σ (<i>I</i>)]R ₁ ^a , wR ₂ ^b	0.0293, 0.0765	0.0396, 0.1211
R(all data)	0.0355	0.0566
GOF ^c on F ²	1.289	1.011
Residual electron Density, e/Å ⁻³	-0.63, 0.57	-0.82, 0.68

$$^a R_1 = \sum ||F_o| - |F_c|| / \sum |F_o|, ^b wR_2 (F_o^2) = [\sum [w(F_o^2 - F_c^2)^2] / \sum w F_o^4]^{1/2} \text{ and } ^c \text{GOF} = [\sum [w(F_o^2 - F_c^2)^2] / (N_{\text{obs}} - N_{\text{params}})]^{1/2}$$

Table 2: Photosensitivity of complexes **1** and **2** obtained from I-V curve.View Article Online
DOI: 10.1039/D0NJ03325A

Complex	Condition	Leakage current		Ratio	Photosensitivity I_{Ph}/I_D
		Reverse	Forward		
1	dark	3.46×10^{-8}	8.4×10^{-8}	2.42	1.13
1	light	5.39×10^{-8}	1.48×10^{-7}	2.74	
2	dark	3.42×10^{-4}	8.13×10^{-4}	2.37	5.41
2	light	1.16×10^{-4}	1.49×10^{-3}	12.84	

Table 3: Device parameters for complex **1**.

Condition	On/off	conductivity δ	ideality factor η	$dv/dlnI$ Rs	H Rs	barrier height Φ_B
dark	2.34	13.1×10^{-8}	2.58	7	8.7	0.67
light	2.89	11.2×10^{-7}	1.46	2.58	3.46	0.41

Table 4: Device parameter for complex **2**.

Condition	on /off	conductivity δ	ideality factor η	dv/dl nI Rs	H Rs	barrier height Φ_B	life time t (s)	D $\times 10^{-11}$	L_D $\times 10^{-5}$	mobility μ_{eff} $\times 10^{-8}$
dark	2.3	5.4×10^{-8}	2.5	25.26	24.37	0.63	1.96	292.6	3.38	8.78
light	13	13.5×10^{-7}	1.24	8.21	7.48	0.32	1.31	49.8	1.14	1.495

Table of Contents Only

View Article Online
DOI: 10.1039/D0NJ03325A**Tetra- and poly-nuclear Cd(II) complexes of an N₃O₄ Schiff base ligand: Crystal structures, electrical conductivity and photoswitching property**Tanmoy Kumar Ghosh,^a Sumanta Jana,^b Subrata Jana^a and Ashutosh Ghosh^{a*}

A tetranuclear and a polymeric Cd(II) complex have been synthesized and characterized. The polymeric complex based device behaves as Schottky Barrier Diode and exhibits photoswitching property.

